

Doping evolution of superconductivity, charge order and band topology in hole-doped topological kagome superconductors $\text{Cs}(\text{V}_{1-x}\text{Ti}_x)_3\text{Sb}_5$

Yixuan Liu,^{1,2,*} Yuan Wang,^{1,2,*} Yongqing Cai,^{1,2,*} Zhanyang Hao,^{1,2,*} Xiao-Ming Ma,^{1,2} Le Wang,^{1,2} Cai Liu,^{1,2} Jian Chen,¹ Liang Zhou,¹ Jinhua Wang,¹ Shanming Wang,¹ Hongtao He,¹ Yi Liu,³ Shengtao Cui,³ Jianfeng Wang,^{4,5,†} Bing Huang,⁵ Chaoyu Chen,^{1,2,‡} and Jia-Wei Mei^{1,2,6,§}

¹*Shenzhen Institute for Quantum Science and Engineering, and Department of Physics, Southern University of Science and Technology, Shenzhen 518055, China*

²*International Quantum Academy, and Shenzhen Branch, Hefei National Laboratory, Futian District, Shenzhen 518048, China*

³*National Synchrotron Radiation Laboratory, University of Science and Technology of China, Hefei 230029, China*

⁴*School of Physics, Beihang University, Beijing 100191, China*

⁵*Beijing Computational Science Research Center, Beijing 100193, China*

⁶*Shenzhen Key Laboratory of Advanced Quantum Functional Materials and Devices, Southern University of Science and Technology, Shenzhen 518055, China*

(Dated: January 23, 2022)

The newly discovered Kagome superconductors AV_3Sb_5 ($A = \text{K}, \text{Rb}, \text{Cs}$) exhibit superconductivity, charge order, and band topology simultaneously. To explore the intricate interplay between the superconducting and charge orders, we investigate the doping evolution of superconductivity, charge-density-wave (CDW) order and band topology in doped topological kagome superconductors $\text{Cs}(\text{V}_{1-x}\text{Ti}_x)_3\text{Sb}_5$ where the Ti-dopant introduces hole-like charge carriers. Despite the absence of the CDW phase transition in doped compounds even for the lowest doping level of $x = 0.047$, the superconductivity survives in all doped samples with enhanced critical temperatures. The high-resolution angle-resolved photoemission spectroscopy (ARPES) measurements reveal that the Ti-dopant in the kagome plane lowers the chemical potential, pushing the van Hove singularity (VHS) at M point above the Fermi level. First-principle simulations corroborate the doping evolution of the band structure observed in ARPES, and affirm that the CDW instability does not occur once the VHS is pushed above the Fermi level, explaining the absence of the CDW ordering in our doped samples $\text{Cs}(\text{V}_{1-x}\text{Ti}_x)_3\text{Sb}_5$. Our results demonstrate a competition between the CDW and superconducting orders in the kagome-metal superconductor CsV_3Sb_5 , although the superconductivity is likely inconsequential of the CDW order.

The transition-metal kagome compounds host novel correlated and topological electronic states and have been catching lots of attention in recent years [1–11]. Due to the geometrical frustration for electron hoppings, the simple kagome-lattice band structure possesses Dirac cones, flat band, and saddle point with van Hove singularities (VHS) in the electronic density of states (DOS), facilitating the emergence of various electronic orders [1–3, 12–14]. Among the kagome metal compounds, the charge-density-wave (CDW) charge order and superconductivity arise successively at around 78–103 K and 0.92–2.5 K, respectively, and intertwine with each other at low temperatures in the AV_3Sb_5 ($A = \text{K}, \text{Rb}, \text{Cs}$) family [9–11, 15, 16], provoking hot topics of recent interests. The angle-resolved-photoemission spectroscopy (ARPES) also reveals a band topology with multiple Dirac lines and loops and a rich nature of VHSs close to the Fermi level in AV_3Sb_5 [10, 17–24].

The CDW order in AV_3Sb_5 ($A = \text{K}, \text{Rb}, \text{Cs}$) is a 2×2 three-dimensional one with unconventional properties [17, 18, 25–29]. Although the muon spin spectroscopy measurement does not detect any local moment for the vanadium ions [30], a giant anomalous Hall conductivity was observed [31, 32] below the CDW transition temperature, implying a non-trivial chirality with the time-reversal symmetry breaking [27–29]. The scanning tunneling microscope/spectroscopy reveals nematic/sematic order and pairing-density-wave order in CsV_3Sb_5 [15, 16], by interesting analogy with

intertwined orders in the high-temperature cuprate superconductors [33, 34]. The CDW order can be completely suppressed under low pressures with emerging the superconducting domes [35–37], implying a competition between the CDW order and the superconductivity [38]. The fragility of CDW against pressures suggests that the electronic structure determines its nature, however, no ARPES measurement of the band structure in response to external perturbations has been reported.

In this letter, we substitute vanadium with titanium in CsV_3Sb_5 to modulate the chemical potential and study the doping evolution of superconductivity, charge order and band topology in $\text{Cs}(\text{V}_{1-x}\text{Ti}_x)_3\text{Sb}_5$. We do not observe the CDW phase transition in the doped compounds even for the doping level of $x = 0.047$ in the transport and thermodynamic measurements. Meanwhile, the superconductivity remains with an enhanced temperature in all doped samples. From the ARPES measurements, we reveal that the overall pattern of band structures remains unchanged upon doping, but the Fermi level lowers down and hence the VHS1 at the M point (Fig. 3) rises up in $\text{Cs}(\text{V}_{1-x}\text{Ti}_x)_3\text{Sb}_5$. Our first-principles simulations confirm the band evolution upon doping and affirm that the CDW instability in the parent compound [39] does not occur once VHS1 is pushed above the Fermi level, accounting for the absence of CDW in the doped samples. Except for the parent compound, the superconducting temperature T_c decreases with increasing the doping levels, coinciding with the DOS of

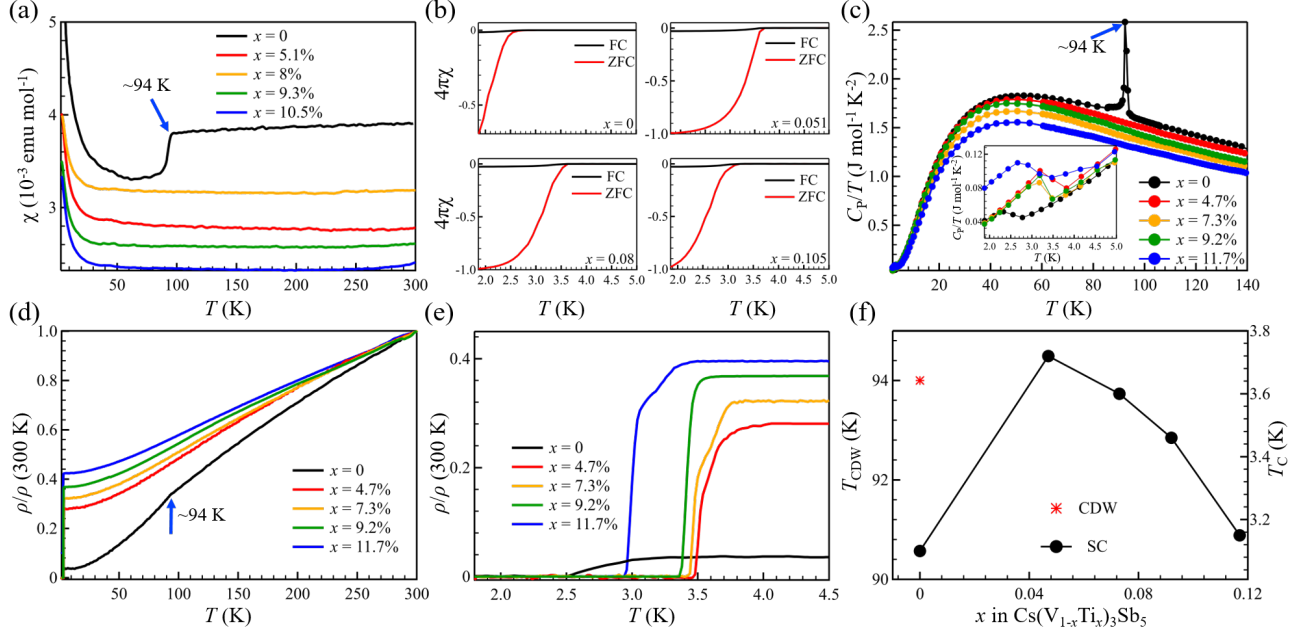


FIG. 1. Thermodynamic and transport properties of $\text{Cs}(\text{V}_{1-x}\text{Ti}_x)_3\text{Sb}_5$. (a) Temperature-dependent uniform magnetic susceptibilities $\chi = M/H$ with the c -axis directional field $H = 10^4$ Oe. (b) The zero-field-cool (ZFC) and field-cool (FC) magnetic susceptibility data under $H = 20$ Oe. (c) Temperature-dependent specific heat coefficient C_p/T at zero field. The inset is the zoom-in low temperature data. (d) Temperature-dependent resistivity ρ with respect to the 300 K result. (e) The zoom-in low temperature data of (d). (f) The doping dependent CDW and superconducting transition temperatures.

the Sb-derived electron pocket at Γ point. The parent compound has a larger DOS of the Sb electron pocket, but a lower T_c than the doped samples, indicating a competition between the CDW order and the superconductivity.

$\text{Cs}(\text{V}_{1-x}\text{Ti}_x)_3\text{Sb}_5$ single crystals with the titanium doping were synthesized by the self-flux method with the starting ratio $\text{Cs} : \text{V} : \text{Ti} : \text{Sb} = 2 : 1 : x_{\text{Ti}} : 6$ for $0 \leq x_{\text{Ti}} \leq 0.5$ [40]. The chemical composition of $\text{Cs}(\text{V}_{1-x}\text{Ti}_x)_3\text{Sb}_5$ was identified by Energy Dispersive X-Ray Spectroscopy (EDX, Phenom ProX). Fig. 1 summarizes the thermodynamic and transport properties of $\text{Cs}(\text{V}_{1-x}\text{Ti}_x)_3\text{Sb}_5$ with different doping levels x . Titanium sits on the left next to vanadium, and the substitution reduces the total number of charge carriers. The lowest doping concentration with $x = 0.047$ of our samples already completely suppresses the CDW transition. However, the superconducting state at low temperatures survives at all doping levels ($0.047 \leq x \leq 0.117$) with enhanced critical temperatures. In Fig. 1(a), we compare the temperature-dependent magnetic susceptibilities of the parent compound CsV_3Sb_5 and the Ti-doped ones $\text{Cs}(\text{V}_{1-x}\text{Ti}_x)_3\text{Sb}_5$. A sudden drop of the magnetization in CsV_3Sb_5 appears at 94 K, indicating the CDW transition [9]. For all Ti-doped samples, no CDW anomaly occurs, implying the absence of the CDW transition. We observe increasingly weakened magnetization signature at both high and low temperatures with the increasing doping levels x , suggesting a reduction of DOS of itinerant electrons or local correlations for vanadium 3d electrons upon doping. The complete suppression of CDW is also

revealed in the heat capacity and the resistivity measurements in Figs. 1(c) and (d)-(e). All the samples of $\text{Cs}(\text{V}_{1-x}\text{Ti}_x)_3\text{Sb}_5$ display the superconducting transition at low temperatures in the magnetization (Fig. 1(b)), heat capacity (Fig. 1(c)) and resistivity (Fig. 1(d)-(e)) measurements. Fig. 1(f) is the doping-dependent transition temperatures of the CDW order and the superconductivity.

High-resolution ARPES measurements are performed to investigate the band structure evolution of the $\text{Cs}(\text{V}_{1-x}\text{Ti}_x)_3\text{Sb}_5$ with different doping level. As detailed photon energy dependent ARPES measurements have been performed [24], the value of k_z can be determined precisely. Fig. 2(a) shows band structures measured at 17 K of different doping level with 31 eV photons, which correspond to the A-H-L plane ($k_z = \pi$). As we can see, an electron-like band around A, several Dirac cone-like dispersions along the A-H-L direction can be clearly resolved in this system. To focus on how these bands evolve with different doping, we extract the their band dispersions by fitting the momentum distribution curves (MDCs), marked by A-D in different colors, and then draw them in Fig. 2(b) separately. The overall band structures shift upwards with different doping level monotonously, in accordance with the fact that hole doping pushes the Fermi level (E_F) downwards. By substituting 11% percent of V atoms with Ti atoms, the band structure can be shifted up about 100 meV. Our results prove that the substitution of Ti is an efficient way to tune the Fermi level of CsV_3Sb_5 system.

As shown in Fig. 1, there is no CDW anomaly for all the

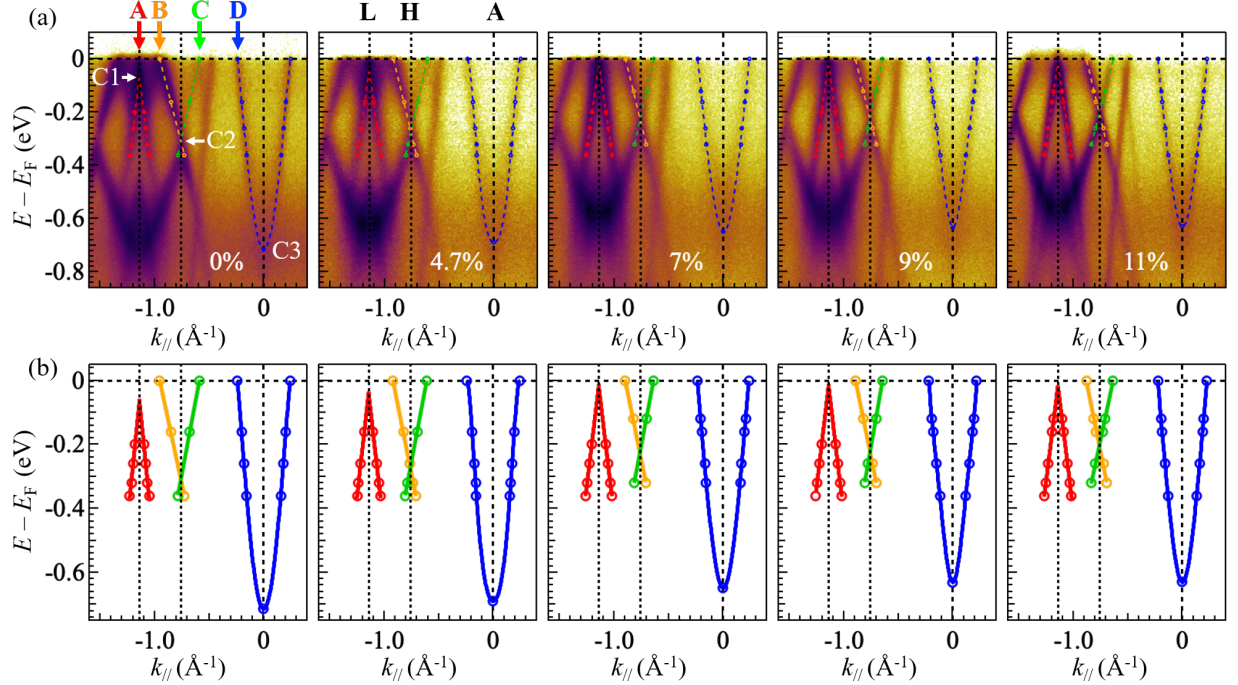


FIG. 2. The doping evolution of the electronic structures of $\text{Cs}(\text{V}_{1-x}\text{Ti}_x)_3\text{Sb}_5$. (a) Band structures measured along the A-H-L directions with 31 eV photons at 17 K with different doping levels. (b) The corresponding schematic band dispersions extracted from (a).

Ti-doped CsV_3Sb_5 compounds. Since the VHSs at the M point near the Fermi level play crucial roles in the CDW instability, it is of importance to figure out how the VHSs near the Fermi level evolve with different doping. We select three typical doping levels ($x = 0, 0.047$ and 0.11) and analyse their detailed band structures around the L point, as shown in Figs. 3(a-c). According to the previous ARPES study [24], the ARPES spectral intensity is dominated by contribution from only the top two layers, resulting in the lack of clear k_z dispersion along M-L and the missing information of the VHSs around the M point. To have a fully clear understanding on the evolutions of band structure and VHSs upon doping, first-principles simulations within density-functional theory (DFT) are performed here [40]. As revealed by ARPES measurements in Fig. 2, except for the overall upward shift, all the features of band structure remains almost unchanged under doping, meaning that the Ti-dopant doesn't break any crystal symmetry of CsV_3Sb_5 . Therefore, we employ a virtual crystal approximation in the simulations of Ti-substituted V in CsV_3Sb_5 , which is qualitatively consistent with the results calculated using the supercell of $\text{Cs}(\text{V}_{1-x}\text{Ti}_x)_3\text{Sb}_5$ [40]. Fig. 3(a) demonstrates that the DFT calculated band structure can well fit the ARPES measurements of CsV_3Sb_5 . As shown in Fig. 3(d), upon doping of Ti, the overall band structures are shifted upwards, consistent with the hole-doped effect revealed by ARPES. Now we focus on the evolutions of VHSs. Around the Fermi level, there are two VHSs (VHS1 and VHS2) at both the M and L points, as marked by red arrows in Fig. 3(d). It is noted that the VHS1 has a large k_z

dispersion along M-L, and it crosses the Fermi level from the M (below E_F) to L (above E_F) points, as shown in Fig. 3(e). While the VHS2 has almost no k_z dispersion along M-L. In addition, the VHS1 has a higher density of states (DOS) near E_F , which accounts for the CDW instability as will be demonstrated below.

Around the L point, the VHS1 cannot be measured by ARPES due to $E(\text{VHS1}) > E_F$, but the VHS2 is observed under all our doping levels, as shown in Figs. 3(a-c). We extract the band dispersions around VHS2 [red circles in Figs. 3(a-c)] and fit them with red dashed lines. Thus the exact positions of VHS2 can be obtained quantitatively. In Fig. 3(f), we summarize the calculated and experimental energy shifts of these two VHSs under different doping levels where both the energies of VHS1 at M and L are plotted here. In general, all the energies of VHSs are shifted upward with respect to E_F as increasing doping level. The calculated energy evolution of VHS2 [green circles in Fig. 3(f)] is in good agreement with the experimental results [blue stars in Fig. 3(f)]. Focusing on the VHS1, its k_z dispersion along M-L allows the VHS1 to be located at any energy position between the energies of the M and L points, which has been plotted by the cyan region in Fig. 3(f). In other words, the VHS1 can be in principle located at any position of the cyan region except for some energy gaps caused by the coupling between VHS1 and other bands. It is noted that the CDW instability is mainly induced by the VHS at E_F . Therefore, that the Fermi energy is included in the range of VHS1 energy between the M and L points is a necessary condition for the formation of CDW. As shown in Fig. 3(f), for

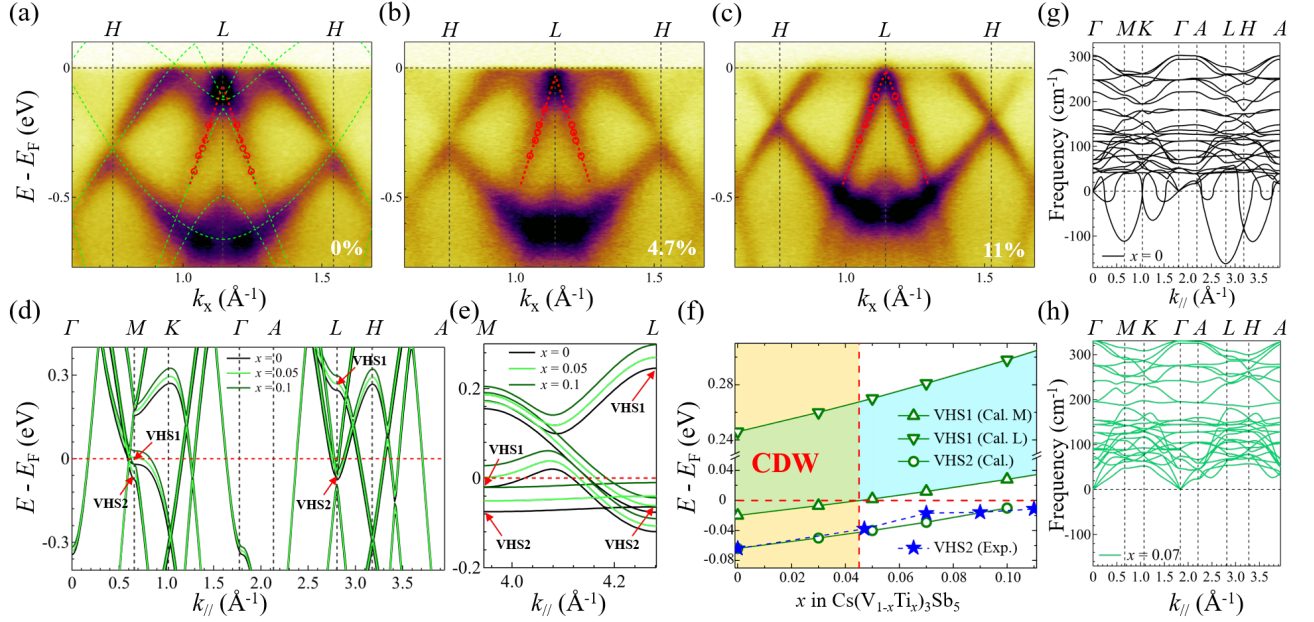


FIG. 3. Doping evolution of VHSs at the M/L points in $\text{Cs}(\text{V}_{1-x}\text{Ti}_x)_3\text{Sb}_5$. (a)-(c) ARPES measurements along the H-L-H direction with selected doping levels. In (a) the DFT calculated band structure (green dashed lines) is also over-plotted. The DFT calculated projected bulk band structure along Γ -M-K- Γ and A-L-H-A directions in (d) and along the M-L direction in (e). (f) The comparison between the calculated and experimental results on the energy shift of VHSs with doping. (g-h) The calculated phonon dispersion relations with doping level $x = 0$ (g) and $x = 0.07$ (h).

the parent compound CsV_3Sb_5 , the VHS1 at M (L) is below (above) E_F . With hole doping, the VHS1 at M shifts upward and is pushed above the Fermi level beyond 4.5% doping concentration ($x > 0.045$). As a consequence, we can divide the phase diagram by $x = 0.045$. When $x < 0.045$, the VHS1 can be located at the Fermi level, and the CDW order may be formed. When $x > 0.045$, all the energy of VHS1 is above the Fermi level, and the CDW order is hard to form. This result can well explain why no CDW anomaly occurs for all the $\text{Cs}(\text{V}_{1-x}\text{Ti}_x)_3\text{Sb}_5$ compounds with $x \geq 0.047$. As demonstrated by previous study [39], the CDW instability can be identified by the imaginary frequency of the phonon spectrum. Here, we compare the calculated phonon spectrum under different doping level with $x = 0$ and $x = 0.07$, as shown in Figs. 3(g,h). For the undoped CsV_3Sb_5 , unstable modes with imaginary frequencies exist at M and L. For the 7% doping concentration, these unstable modes disappear, which implies the absence of the CDW order. Combining all the results above, it can be concluded that the hole doping pushes the VHS1 above the Fermi level, and then lead to the disappearance of the CDW instabilities. Our results also reveal that the VHS1 plays a dominant role in the formation of the CDW order.

The very different doping behaviors in $\text{Cs}(\text{V}_{1-x}\text{Ti}_x)_3\text{Sb}_5$ suggest that the CDW and the superconducting orders in the parent compound have different underlying electronic origins. Our results affirm the VHS saddle point on the V bands leads to the CDW instability, consistent with the pre-

vious theory [39]. However, it is unlikely the reason for the superconductivity since T_c survives even when the doping of Ti pushes VHS1 above the Fermi level, at odds with the previous speculation of the nature of pairing around the VHS [41]. Recent NMR and magnetic penetration depth measurements [42, 43] suggest a conventional s -wave superconducting pairing in CsV_3Sb_5 , which unlikely occurs on the V bands regarding the robustness of the superconductivity upon

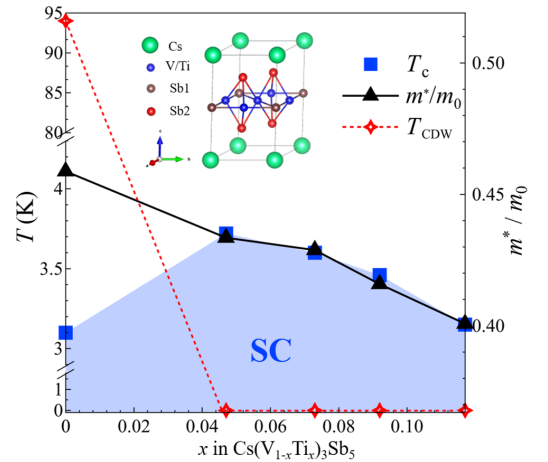


FIG. 4. Doping evolution of the CDW order T_{cdw} , superconducting transition temperatures T_c and effective mass m^* of the Sb-derived electron pockets at Γ of $\text{Cs}(\text{V}_{1-x}\text{Ti}_x)_3\text{Sb}_5$.

doping in $\text{Cs}(\text{V}_{1-x}\text{Ti}_x)_3\text{Sb}_5$. To investigate the relationship between the superconductivity and the Sb electron pocket, we compare the effective mass (m^*) of the Sb electron pocket at the Γ point (C3 band in Fig. 2) with the superconducting transition temperatures T_c . Due to the quasi-2D structure, m^* is proportional to DOS, and its doping evolution agrees well with T_c in $\text{Cs}(\text{V}_{1-x}\text{Ti}_x)_3\text{Sb}_5$ except the parent compound, as shown in Fig. 4. The similar doping behaviors of m^* and T_c in the doped samples imply a BCS scenario, consistent with the s -wave pairing [42, 43]. The parent compound has the largest effective mass m^* , but with a suppressed T_c , consistent with the competition relationship between the CDW order and the superconductivity [15, 16, 35–38].

In conclusion, the doping evolution of the band structures in $\text{Cs}(\text{V}_{1-x}\text{Ti}_x)_3\text{Sb}_5$ manifests that the van Hove singularity is the origin of the CDW ordering, but not of the superconductivity which likely occurs on the Sb electron pocket. Although they have different origins, the charge order and the superconductivity displays a competition relation, accounting for the intertwined orders in the parent compound CsV_3Sb_5 .

This work is supported by National Natural Science Foundation of China (NSFC) (Grants Nos. 12074163 and 12004030), the Shenzhen High-level Special Fund (Grants No. G02206304 and No. G02206404), the Guangdong Innovative and Entrepreneurial Research Team Program (Grants No. 2017ZT07C062 and No. 2019ZT08C044), Shenzhen Science and Technology Program (Grant No. KQTD20190929173815000), the University Innovative Team in Guangdong Province (No. 2020KCXTD001), Shenzhen Key Laboratory of Advanced Quantum Functional Materials and Devices (No. ZDSYS20190902092905285), Guangdong Basic and Applied Basic Research Foundation (No. 2020B1515120100), and China Postdoctoral Science Foundation (2020M682780).

* These authors contributed equally.

† wangjf06@buaa.edu.cn

‡ chency@sustech.edu.cn

§ meijw@sustech.edu.cn

- [1] S. V. Isakov, S. Wessel, R. G. Melko, K. Sengupta, and Y. B. Kim, Hard-core bosons on the kagome lattice: Valence-bond solids and their quantum melting, *Phys. Rev. Lett.* **97**, 147202 (2006).
- [2] H.-M. Guo and M. Franz, Topological insulator on the kagome lattice, *Phys. Rev. B* **80**, 113102 (2009).
- [3] E. Tang, J.-W. Mei, and X.-G. Wen, High-temperature fractional quantum hall states, *Phys. Rev. Lett.* **106**, 236802 (2011).
- [4] S. Nakatsuji, N. Kiyohara, and T. Higo, Large anomalous hall effect in a non-collinear antiferromagnet at room temperature, *Nature* **527**, 212 (2015).
- [5] E. Liu, Y. Sun, N. Kumar, L. Muechler, A. Sun, L. Jiao, S.-Y. Yang, D. Liu, A. Liang, Q. Xu, J. Kroder, V. Süß, H. Borrmann, C. Shekhar, Z. Wang, C. Xi, W. Wang, W. Schnelle, S. Wirth, Y. Chen, S. T. B. Goennenwein, and C. Felser, Giant anomalous hall effect in a ferromagnetic kagome-lattice semimetal, *Nature Physics* **14**, 1125 (2018).
- [6] L. Ye, M. Kang, J. Liu, F. von Cube, C. R. Wicker, T. Suzuki, C. Jozwiak, A. Bostwick, E. Rotenberg, D. C. Bell, L. Fu, R. Comin, and J. G. Checkelsky, Massive dirac fermions in a ferromagnetic kagome metal, *Nature* **555**, 638 (2018).
- [7] F. Liu D., J. Liang A., K. Liu E., N. Xu Q., W. Li Y., C. Chen, D. Pei, J. Shi W., K. Mo S., P. Dudin, T. Kim, C. Cacho, G. Li, Y. Sun, X. Yang L., K. Liu Z., P. Parkin S. S., C. Felser, and L. Chen Y., Magnetic weyl semimetal phase in a kagomé crystal, *Science* **365**, 1282 (2019).
- [8] J.-X. Yin, W. Ma, T. A. Cochran, X. Xu, S. S. Zhang, H.-J. Tien, N. Shumiya, G. Cheng, K. Jiang, B. Lian, Z. Song, G. Chang, I. Belopolski, D. Multer, M. Litskevich, Z.-J. Cheng, X. P. Yang, B. Swidler, H. Zhou, H. Lin, T. Neupert, Z. Wang, N. Yao, T.-R. Chang, S. Jia, and M. Zahid Hasan, Quantum-limit chern topological magnetism in TbMn_6Sn_6 , *Nature* **583**, 533 (2020).
- [9] B. R. Ortiz, L. C. Gomes, J. R. Morey, M. Winiarski, M. Bordenon, J. S. Mangum, I. W. H. Oswald, J. A. Rodriguez-Rivera, J. R. Neilson, S. D. Wilson, E. Ertekin, T. M. McQueen, and E. S. Toberer, New kagome prototype materials: discovery of KV_3Sb_5 , RbV_3Sb_5 , and CsV_3Sb_5 , *Phys. Rev. Materials* **3**, 094407 (2019).
- [10] B. R. Ortiz, S. M. L. Teicher, Y. Hu, J. L. Zuo, P. M. Sarte, E. C. Schueller, A. M. M. Abeykoon, M. J. Krogstad, S. Rosenkranz, R. Osborn, R. Seshadri, L. Balents, J. He, and S. D. Wilson, CsV_3Sb_5 : A \mathbb{Z}_2 topological kagome metal with a superconducting ground state, *Phys. Rev. Lett.* **125**, 247002 (2020).
- [11] B. R. Ortiz, P. M. Sarte, E. M. Kenney, M. J. Graf, S. M. L. Teicher, R. Seshadri, and S. D. Wilson, Superconductivity in the F_2 kagome metal KV_3Sb_5 , *Phys. Rev. Materials* **5**, 034801 (2021).
- [12] M. D. Johannes and I. I. Mazin, Fermi surface nesting and the origin of charge density waves in metals, *Phys. Rev. B* **77**, 165135 (2008).
- [13] W.-S. Wang, Z.-Z. Li, Y.-Y. Xiang, and Q.-H. Wang, Competing electronic orders on kagome lattices at van hove filling, *Phys. Rev. B* **87**, 115135 (2013).
- [14] M. L. Kiesel, C. Platt, and R. Thomale, Unconventional fermi surface instabilities in the kagome hubbard model, *Phys. Rev. Lett.* **110**, 126405 (2013).
- [15] H. Chen, H. Yang, B. Hu, Z. Zhao, J. Yuan, Y. Xing, G. Qian, Z. Huang, G. Li, Y. Ye, S. Ma, S. Ni, H. Zhang, Q. Yin, C. Gong, Z. Tu, H. Lei, H. Tan, S. Zhou, C. Shen, X. Dong, B. Yan, Z. Wang, and H.-J. Gao, Roton pair density wave in a strong-coupling kagome superconductor, *Nature* **10.1038/s41586-021-03983-5** (2021).
- [16] H. Zhao, H. Li, B. R. Ortiz, S. M. L. Teicher, T. Park, M. Ye, Z. Wang, L. Balents, S. D. Wilson, and I. Zeljkovic, Cascade of correlated electron states in a kagome superconductor CsV_3Sb_5 , *Nature* **10.1038/s41586-021-03946-w** (2021).
- [17] H. Luo, Q. Gao, H. Liu, Y. Gu, D. Wu, C. Yi, J. Jia, S. Wu, X. Luo, Y. Xu, L. Zhao, Q. Wang, H. Mao, G. Liu, Z. Zhu, Y. Shi, K. Jiang, J. Hu, Z. Xu, and X. J. Zhou, Electronic nature of charge density wave and electron-phonon coupling in kagome superconductor KV_3Sb_5 (2021), [arXiv:2107.02688](https://arxiv.org/abs/2107.02688) [cond-mat.supr-con].
- [18] H. Li, T. T. Zhang, T. Yilmaz, Y. Y. Pai, C. E. Marvinney, A. Said, Q. W. Yin, C. S. Gong, Z. J. Tu, E. Vescovo, C. S. Nelson, R. G. Moore, S. Murakami, H. C. Lei, H. N. Lee, B. J. Lawrie, and H. Miao, Observation of unconventional charge density wave without acoustic phonon anomaly in kagome superconductors AV_3Sb_5 ($A = \text{Rb}, \text{Cs}$), *Phys. Rev. X* **11**, 031050 (2021).
- [19] M. Kang, S. Fang, J.-K. Kim, B. R. Ortiz, J. Yoo, B.-G. Park,

- S. D. Wilson, J.-H. Park, and R. Comin, Twofold van hove singularity and origin of charge order in topological kagome superconductor CsV_3Sb_5 (2021), [arXiv:2105.01689 \[cond-mat.str-el\]](#).
- [20] R. Lou, A. Fedorov, Q. Yin, A. Kuibarov, Z. Tu, C. Gong, E. F. Schwier, B. Büchner, H. Lei, and S. Borisenko, Charge-density-wave-induced peak-dip-hump structure and flat band in the kagome superconductor CsV_3Sb_5 (2021), [arXiv:2106.06497 \[cond-mat.supr-con\]](#).
- [21] S. Cho, H. Ma, W. Xia, Y. Yang, Z. Liu, Z. Huang, Z. Jiang, X. Lu, J. Liu, Z. Liu, J. Jia, Y. Guo, J. Liu, and D. Shen, Emergence of new van hove singularities in the charge density wave state of a topological kagome metal RbV_3Sb_5 (2021), [arXiv:2105.05117 \[cond-mat.supr-con\]](#).
- [22] Y. Hu, X. Wu, B. R. Ortiz, S. Ju, X. Han, J. Z. Ma, N. C. Plumb, M. Radovic, R. Thomale, S. D. Wilson, A. P. Schnyder, and M. Shi, Rich nature of van hove singularities in kagome superconductor CsV_3Sb_5 (2021), [arXiv:2106.05922 \[cond-mat.supr-con\]](#).
- [23] Y. Hu, S. M. L. Teicher, B. R. Ortiz, Y. Luo, S. Peng, L. Huai, J. Z. Ma, N. C. Plumb, S. D. Wilson, J. F. He, and M. Shi, Charge-order-assisted topological surface states and flat bands in the kagome superconductor CsV_3Sb_5 (2021), [arXiv:2104.12725 \[cond-mat.supr-con\]](#).
- [24] Y. Cai, Y. Wang, Z. Hao, Y. Liu, X.-M. Ma, Z. Shen, Z. Jiang, Y. Yang, W. Liu, Q. Jiang, Z. Liu, M. Ye, D. Shen, Z. Sun, J. Chen, L. Wang, C. Liu, J. Lin, J. Wang, B. Huang, J.-W. Mei, and C. Chen, Emergence of quantum confinement in topological kagome superconductor CsV_3Sb_5 family (2021), [arXiv:2109.12778 \[cond-mat.str-el\]](#).
- [25] Y. Luo, S. Peng, S. M. L. Teicher, L. Huai, Y. Hu, B. R. Ortiz, Z. Wei, J. Shen, Z. Ou, B. Wang, Y. Miao, M. Guo, M. Shi, S. D. Wilson, and J. F. He, Distinct band reconstructions in kagome superconductor CsV_3Sb_5 (2021), [arXiv:2106.01248 \[cond-mat.str-el\]](#).
- [26] Z. Liang, X. Hou, F. Zhang, W. Ma, P. Wu, Z. Zhang, F. Yu, J.-J. Ying, K. Jiang, L. Shan, Z. Wang, and X.-H. Chen, Three-dimensional charge density wave and surface-dependent vortex-core states in a kagome superconductor CsV_3Sb_5 , *Phys. Rev. X* **11**, 031026 (2021).
- [27] Y.-X. Jiang, J.-X. Yin, M. M. Denner, N. Shumiya, B. R. Ortiz, G. Xu, Z. Guguchia, J. He, M. S. Hossain, X. Liu, J. Ruff, L. Kautzsch, S. S. Zhang, G. Chang, I. Belopolski, Q. Zhang, T. A. Cochran, D. Multer, M. Litskevich, Z.-J. Cheng, X. P. Yang, Z. Wang, R. Thomale, T. Neupert, S. D. Wilson, and M. Z. Hasan, Unconventional chiral charge order in kagome superconductor KV_3Sb_5 , *Nature Materials* **20**, 1353 (2021).
- [28] X. Feng, K. Jiang, Z. Wang, and J. Hu, Chiral flux phase in the kagome superconductor AV_3Sb_5 , *Science Bulletin* **66**, 1384 (2021).
- [29] M. M. Denner, R. Thomale, and T. Neupert, Analysis of charge order in the kagome metal AV_3Sb_5 ($A = \text{K}, \text{Rb}, \text{Cs}$) (2021), [arXiv:2103.14045 \[cond-mat.str-el\]](#).
- [30] E. M. Kenney, B. R. Ortiz, C. Wang, S. D. Wilson, and M. J. Graf, Absence of local moments in the kagome metal KV_3Sb_5 as determined by muon spin spectroscopy, *Journal of Physics: Condensed Matter* **33**, 235801 (2021).
- [31] S.-Y. Yang, Y. Wang, B. R. Ortiz, D. Liu, J. Gayles, E. Derunova, R. Gonzalez-Hernandez, L. Šmejkal, Y. Chen, S. S. P. Parkin, S. D. Wilson, E. S. Toberer, T. McQueen, and M. N. Ali, Giant, unconventional anomalous Hall effect in the metallic frustrated magnet candidate, KV_3Sb_5 , *Science Advances* **6**, eabb6003 (2020).
- [32] F. H. Yu, T. Wu, Z. Y. Wang, B. Lei, W. Z. Zhuo, J. J. Ying, and X. H. Chen, Concurrence of anomalous hall effect and charge density wave in a superconducting topological kagome metal, *Phys. Rev. B* **104**, L041103 (2021).
- [33] E. Fradkin, S. A. Kivelson, and J. M. Tranquada, Colloquium: Theory of intertwined orders in high temperature superconductors, *Rev. Mod. Phys.* **87**, 457 (2015).
- [34] Z. Dai, Y.-H. Zhang, T. Senthil, and P. A. Lee, Pair-density waves, charge-density waves, and vortices in high- T_c cuprates, *Phys. Rev. B* **97**, 174511 (2018).
- [35] K. Y. Chen, N. N. Wang, Q. W. Yin, Y. H. Gu, K. Jiang, Z. J. Tu, C. S. Gong, Y. Uwatoko, J. P. Sun, H. C. Lei, J. P. Hu, and J. G. Cheng, Double superconducting dome and triple enhancement of T_c in the kagome superconductor CsV_3Sb_5 under high pressure, *Phys. Rev. Lett.* **126**, 247001 (2021).
- [36] F. Du, S. Luo, B. R. Ortiz, Y. Chen, W. Duan, D. Zhang, X. Lu, S. D. Wilson, Y. Song, and H. Yuan, Pressure-induced double superconducting domes and charge instability in the kagome metal KV_3Sb_5 , *Phys. Rev. B* **103**, L220504 (2021).
- [37] F. H. Yu, D. H. Ma, W. Z. Zhuo, S. Q. Liu, X. K. Wen, B. Lei, J. J. Ying, and X. H. Chen, Unusual competition of superconductivity and charge-density-wave state in a compressed topological kagome metal, *Nature Communications* **12**, 3645 (2021).
- [38] S. D. Wilson, Competition under pressure, *Nature Physics* **17**, 885 (2021).
- [39] H. Tan, Y. Liu, Z. Wang, and B. Yan, Charge density waves and electronic properties of superconducting kagome metals, *Phys. Rev. Lett.* **127**, 046401 (2021).
- [40] See Supplementary Materials for thermodynamic, transport and ARPES measurement methods, the calculation methods and the supercell calculations of Ti-doped CsV_3Sb_5 .
- [41] X. Wu, T. Schwemmer, T. Müller, A. Consiglio, G. Sangiovanni, D. Di Sante, Y. Iqbal, W. Hanke, A. P. Schnyder, M. M. Denner, M. H. Fischer, T. Neupert, and R. Thomale, Nature of unconventional pairing in the kagome superconductors ACs_3Sb_5 ($A = \text{K}, \text{Rb}, \text{Cs}$), *Phys. Rev. Lett.* **127**, 177001 (2021).
- [42] C. Mu, Q. Yin, Z. Tu, C. Gong, H. Lei, Z. Li, and J. Luo, S-wave superconductivity in kagome metal CsV_3Sb_5 revealed by $^{121}/^{123}\text{Sb}$ NQR and ^{51}V NMR measurements, *Chinese Physics Letters* **38**, 077402 (2021).
- [43] W. Duan, Z. Nie, S. Luo, F. Yu, B. R. Ortiz, L. Yin, H. Su, F. Du, A. Wang, Y. Chen, X. Lu, J. Ying, S. D. Wilson, X. Chen, Y. Song, and H. Yuan, Nodeless superconductivity in the kagome metal CsV_3Sb_5 , *Science China Physics, Mechanics & Astronomy* **64**, 107462 (2021).